Molecularly Imprinted Polymers Based Surface Plasmon Resonance Sensor for Sulfamethoxazole Detection

Önder KURÇ and Deniz TÜRKMEN*

Department of Chemistry, Hacettepe University, Ankara 06800, Turkey

*Corresponding author: Deniz TÜRKMEN E-mail: denizt@hacettepe.edu.tr

Abstract: Sulfamethoxazole (SMX) is a sulfonamide antibiotic primarily used to treat urinary tract infections and used in veterinary and industrialized husbandry to treat diseases and food additives. Like other antibiotics, SMX is considered as a pollutant in water and food that threaten local life. This study developed a surface plasmon resonance (SPR) sensor chip that is fast, highly selective, and reusable, and requires no pretreatment for detecting SMX. As a receptor, SMX imprinted methacrylic acid-2-hydroxyethyl methacrylate-ethylene glycol dimethacrylate polymer [poly(MAA-HEMA-EGDMA)] was used. The surface of the gold SPR chips was coated with a drop-casting method. The nanofilm coated chips were characterized by scanning electron microscopy (SEM), atomic force microscopy (AFM), ellipsometer, contact angle measurement, and Fourier-transform infrared spectrometry (FTIR). Imprinting factor (IF) was calculated as: ΔR[MIP(molecularly imprinted polymers)]/ΔR[NIP(non-imprinted)]=12/3.5=3.4. Limit of detection (LOD) and limit of quantification (LOQ) values were calculated with 3 s/m and 10 s/m methods, and the results were found to be 0.001 1 μg/L for LOD 0.003 4 μg/L for LOQ. Adsorption studies on both standard SMX solution and commercial milk samples were applied. Also, we investigated the developed chip's reusability, storability, and selectivity with amoxicillin and cefalexin.

Keywords: Antibiotic, sulfamethoxazole, nanofilm chip, molecularly imprinted polymers (MIP), surface plasmon resonance (SPR)

Citation: Önder KURÇ and Deniz TÜRKMEN, "Molecularly Imprinted Polymers Based Surface Plasmon Resonance Sensor for Sulfamethoxazole Detection," *Photonic Sensors*, 2022, 12(4): 220417.

1. Introduction

Sulfamethoxazole (SMX) and other antibiotics are chemical agents to treat bacteria-caused diseases. These agents are consumed in large quantities every year [1] to treat health issues for humans and animals. Moreover, animal husbandry is frequently used as a food additive [2–4] to raise production. These agents differentiate between host and bacteria and use fundamental differences between their metabolic pathways. Antibiotics are essential for health, but they also have many drawbacks, such as environmental pollutants [5, 6] and food pollutants [7–9]. Consuming antibiotic residues may cause serious health problems [10–12]; antibiotic resistance [13, 14] is another issue.

To prevent antibiotic and antibiotic residue-related problems, many organizations like World Health Organization (WHO), European Medicines Agency (EMA), and the Food and Drug Administration (FDA) limit the usage of antibiotics and monitor their presence in the environment and food to evaluate their harms. It is essential to detect these compounds in various samples fast and

Received: 22 December 2021 / Revised: 22 February 2022

DOI: 10.1007/s13320-022-0658-5
Article type: Regular

accurately. These determinations are usually made in food and environment laboratories using traditional methods like chromatography [15, 16] and spectroscopy. While those methods have their advantages, as well as many drawbacks, such as training personnel and expensive equipment. They may require long analysis time and preprocessing, which is both labour- and time-consuming.

Alternative to these methods, sensor technologies could be used for chemical analysis [17, 18]. Sensors are generally small devices used to sense changes occurring in their environment. These changes could be pH [19], heat [20], pressure [21], or in this case, a chemical change like the number of antibiotics [22, 23]. These changes can be easily monitored and controlled simultaneously with a sensitive sensor system. This type of sensor is made with three components: a receptor that can sense the environmental difference, a detector that can detect the difference happening at the receptor and convert it to a signal, and a signal reader that can translate the signal received from the detector.

There are many types of receptor type for sensors, such as enzymes [24, 25], aptamers [26, 27], antibodies [28, 29], molecularly imprinted polymers [30, 31], nucleic acids [32], a tissue [33], or a whole cell [34] that could be used as a receptor. There are many receptors to choose from, but selecting a suitable one requires consideration. For example, the affinity and stability of the receptor are essential factors because sensors "sense" the environment with their receptor, and the receptor's ability to detect will significantly affect sensors. Additionally, the receptor will be in touch with the environmental matrix, so the receptor we choose must be stable in the sensor's matrix. While natural receptors such as enzymes, antibodies, and nucleic acids offer good affinity and selectivity, which are primarily fragile outside of their natural conditions [35–37]. Their price is very high, and they could be used as a limited type of analyte.

Molecularly imprinted polymers (MIP) are synthetic receptors. They consist of binding sites/cavities for their imprinted molecules like enzymes and biological receptors. These binding sites/cavities could have a very high binding affinity. While having great affinity (which is the desired property for detection), another advantage of molecularly imprinted polymers depending on the material and synthesized techniques is that they may have excellent stability and cost lower when compared to biological receptors. The molecularly imprinted polymer is considered a good candidate as a receptor for sensors with these properties.

The gold nanoparticles are preferred as an alternative sensing material for increasing the sensor response signal [38]. The gold nanoparticles shift the dip of a surface plasmon resonance (SPR) curve to a higher SPR angle, and the integration of the gold nanoparticles enhances the signal amplification. AuNPs could be synthesized to achieve the advantage of a diversity of effects, such as changes to the refractive index by the particle mass, enhanced surface area, and electromagnetic-field-coupling between the particles' plasmonic properties and the emitted plasmons [39, 40]. These SPR sensors are generally based on noble metal thin films and nanoscale structures, owing to their feature of the higher optical absorption band in the visible-near infrared range of the electromagnetic spectrum [41]. This study developed an MIP-based enhanced-SPR sensor for sulfamethoxazole detection. An MIP film decorated the SPR gold sensor. The polymerization occurred on the surface of the bare gold chip surface. The thin polymer film was homogeneously coated onto the SPR gold chip surface. The thin film provided a very sensitive response. Designed nanofilm provided the close detection area that matched the evanescent field of surface plasmons to monitor the detection signals properly.

There are many methods to detect receptor changes, such as electrochemical changes [42, 43] or

optical changes [44] like SPR. The SPR-based sensor method is based on the analysis of the target molecule with the aid of a ligand covalently bonded to a metallic (e.g., silver or gold) surface. The target molecule to be analyzed with the help of a microfluidic channel is prepared in different concentrations and characterized by interacting with the ligand structure attached to the gold surface. The SPR signal is caused by the change in the refractive index of the metal chip on the sensor surface. Small changes in mass with binding of the target molecule cause a proportional increase in the refractive index. Accordingly, when the target molecule flowing in the microfluidic channel is bound to the attached ligand, it is measured as the change in the resonance angle of the refracted light in Fig. 1. This technique has many advantages, such as no label required for analysis, fast analysis, non-destructive to the analyte, and real-time analysis, which make it a good choice as a detector [45, 46]. With its advantages, SPR sensors have essential applications such as affinity determination and binding constants [47, 48], monitoring [49, 50], and diagnostic [51, 52] and genotype analysis [53]. Because of these advantages, SPR is a frequently used technique in chemistry, molecular biology, biology, and many other fields as a detector.

This study aimed to develop a sensitive, cost-effective, and selective SMX imprinted nanofilm sensor system. SMX analysis was performed in aqueous media and spiked milk samples in the presence of competitive antibiotics.

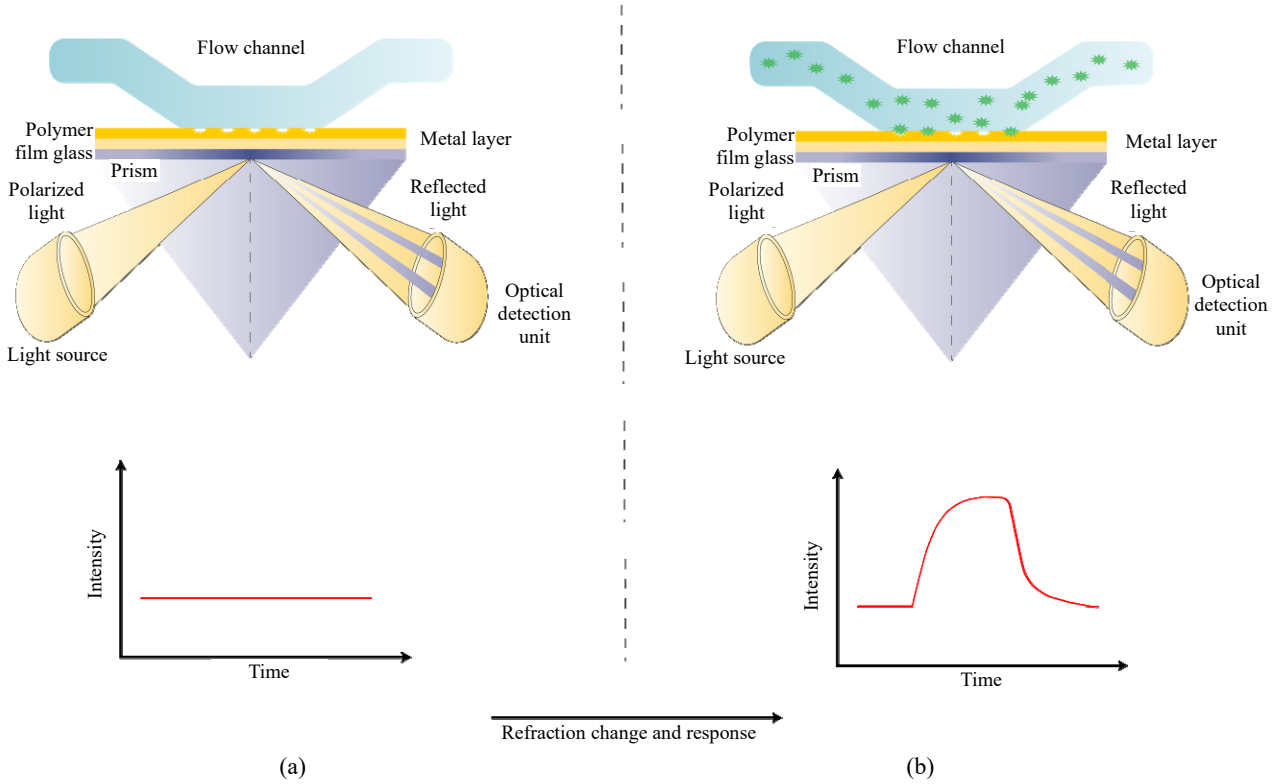

Fig. 1 Principle of SPR system: (a) before interaction (no signal) and (b) after interaction (signal intensity change).

2. Materials and methods

2.1 Materials

The gold SPR chips (product code: SPR-1000-050; chip gold thickness: 50 nm; chip dimensions: 1 mm×18 mm×18 mm; refractive index of glass: 1.72) were purchased from GWC Tech (Madison, USA). SMX, amoxicillin, cephalexin, 2-propene-1-thiol, 2-hydroxyethyl methacrylate (HEMA), ethylene glycol dimethacrylate (EGDMA),

azobisisobutyronitrile, sodium chloride, and methacrylic acid (MAA) were supplied from SIGMA-ALDRICH. All solvents were supplied from Merck KGaA, Darmstadt. The deionized water was purified by Barnstead Deionizer Nanopure Diamond Analytical Water System.

2.2 Design of SMX imprinted chip

The first step was allyl modification of the sensor surface. The second step was preparing SMX-methacrylic acid complex pre complex. In the last step, a nanofilm was prepared by mixing the pre-complex and polymerization mixture on the allyl modified chip surface under appropriate conditions. Before preparing SMX imprinted (SMX-MIP) and non-imprinted (NIP) SPR gold chips, the surfaces of these chips were cleaned by acidic piranha solution (3:1, H_2SO_4:H_2O_2, v/v) for 30 s. They were washed with an aqueous ethanol solution and dried in a vacuum oven at 40 ℃ for 2 hours. After cleaning the surfaces of the chips to form allyl groups on the gold surface of chips, 3 mL of 2.0 mM of the 2-propene-1-thiol solution was dropped on the gold surface of chips and incubated for 2 hours, and then washed with an aqueous ethanol solution to remove 2-propene-1-thiol, not bond the chip surface and dried in a vacuum oven.

The different mole ratios of SMX-methacrylic acid complex (1:0.5, 1:1, 1:2, and 1:3) were examined by the ultraviolet-visible (UV-Vis) spectrophotometer instrument (1240 mini-SHIMADZU, Japan) for choosing the best stoichiometric ratio of SMX and methacrylic acid. The maximum absorbance value was observed in the 1:3 ratio of the SMX-methacrylic acid complex. Therefore, the SMX/methacrylic acid ratio was chosen as 1:3.

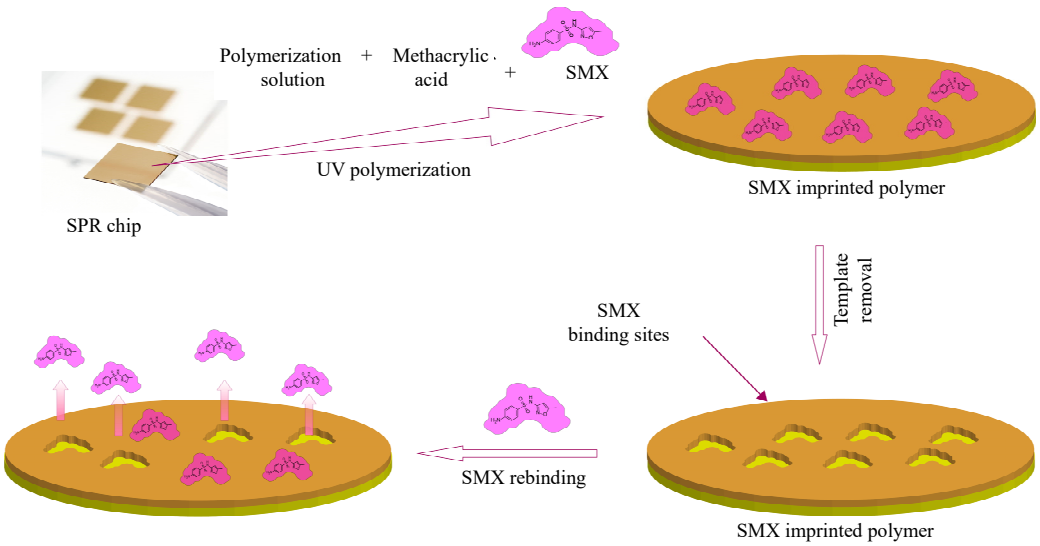

Fig. 2 Schematic representation of SMX-MIP nanofilm preparation.

To prepare the SMX imprinted and nanofilm on the chip surface, a polymerization solution containing 2-hydroxyethyl methacrylate and ethylene glycol dimethacrylate SMX-methacrylic acid complex in 1:3 ratio and azobisisobutyronitrile as initiator was prepared. Then, an aliquot of this solution was dropped on the allyl modified gold surface of the SPR chip. UV light was used at 25 ℃ (100 W and 365 nm) and continued for 1 hour to initiate polymerization in Fig. 2. The non-imprinted film-coated sensor was prepared in the same procedure instead of SMX-methacrylic complex, and methacrylic was added to the polymerization solution. Finally, SMX imprinted and non-imprinted nanofilm modified chips were washed with an aqueous ethanol solution, dried in a vacuum oven, and stored in a vacuum desiccator. Moreover, 0.5 M of the NaOH solution was used to remove SMX

from SMX imprinted nanofilm coated chips. The NIP gold SPR sensor was also designed via the same operation without a template analyte SMX.

2.3 Characterization studies

The SMX imprinted and non-imprinted nanofilm coated chips were characterized by the Fourier transform infrared spectrometer (FTIR), atomic force microscopy (AFM, Nanomagnetics Instruments, UK), scanning electron microscopy (SEM, Tescan, Czechia), ellipsometer (Nanofilm EP3, Germany), and contact angle measurements. FTIR characterization studies of these chips were done by the FTIR-ATR spectrophotometer (Thermo Fisher Scientific, Nicolet is 10, Waltham, USA) in the 400 cm^{-1} – 4 000 cm^{-1} range of wavenumber at a resolution of 2 cm^{-1}. Atomic force microscopy observations were carried out by an ambient AFM (Nanomagnetics Instruments, Oxford, UK) in tapping mode to examine the surfaces deepness. Samples were scanned with 2 μm/s scanning rate at 256×256 pixels resolution. And ellipsometry measurements were carried out by an auto-nulling imaging ellipsometer (Nanofilm EP3, Goettingen, Germany) to examine the thickness value of the polymeric layer on the gold surface of the SPR chip. All thickness measurements had been performed at a wavelength of 658 nm with an incidence angle of 60° and 20× objective. SEM images were taken by focused ion beam scanning electron microscopy (FIB-SEM) (GAIA-3, Tescan). And lastly, contact angle measurements of SMX imprinted and non-imprinted nanofilm coated chips were done using KRUSS DSA100 (Hamburg, Germany).

2.4 Kinetic studies using SMX imprinted SPR nanosensor

Kinetic studies of SMX imprinted and non-imprinted nanosensors were carried out using SPR imager II (GWC, Madison, USA) with 150 μL/min flow rate and 800 nm operating wavelength. SMX performed real-time detection of SMX from an aqueous solution and commercial milk samples imprinted SPR nanosensors. Firstly, detection experiments of SMX from the aqueous solution were performed in different medium pHs (5, 6, 7.4, and 9) to determine the effective medium pH. The detection experiments of SMX from an aqueous solution were done in the range of 0.025 μg/L to 253.2 μg/L. The detection procedure was performed in 20 minutes. The first step of this procedure was equilibration of the sensor by 0.5 M of phosphate buffer, then adsorption of SMX from the SMX solution by the nanosensor, finally desorption of SMX from the nanosensor surface by 0.5 M of NaOH solution. The changes in the resonance frequency were monitored instantly and reached a constant amount in 15 minutes. The selectivity of the SMX imprinted nanosensor was examined using amoxicillin and cephalexin aqueous solutions. The reusability of the SMX imprinted nanosensor was examined by repeating five times of the equilibration-adsorption-desorption cycle by 25.3 μg/L aqueous solutions of SMX.

The detection experiments were performed in commercial milk samples as a real sample to examine the reliability of the prepared SPR nanosensor. The commercial milk samples were centrifuged at 25 000 rpm for 25 minnutes at 4 ℃, then trypsin and Clara-diastase were added to remove the fat layer and hydrolyzed for 30 minnutes at 40 ℃. Finally, after cooling, this solution was centrifuged at 25 000 rpm for 25 minutes and used as a real sample solution.

3. Results and discussion

3.1 Characterizations

The FTIR technique was used to characterise molecularly imprinted and non-molecularly imprinted nanofilms. The first one was acquired from non-imprinted polymers consisting of peaks from the monomer (MAA), cross-linker, and the initiator molecules. The second one acquired from SMX-imprinted polymer-coated chips consists of peaks similar to the non-imprinted polymers expected because of the chemical compounds. Still, the FTIR data of SMX-imprinted chips also had a

peak from the template molecule (SMX). The expected results belonged to our components used in a polymer coating. This showed that the polymerization components caused functional groups, and the polymerization was done correctly.

The FTIR peak at 1 210 cm^{-1} – 1 160 cm^{-1} from carbon-oxygen ester bond (C–O), 1 718 cm^{-1} was from carboxyl groups (C=O) and the last peak at 2 980 cm^{-1} – 2 920 cm^{-1} from the hydroxyl groups (O–H). The FTIR spectrum was acquired from molecular imprinted polymer-coated chips. While some parts of the spectrum were identical to the first spectrum, it also had peaks caused by the template (SMX) molecules. The peak at 1 365 cm^{-1} was caused by sulfonamide groups (S=O), the peak at 1 503 cm^{-1} was from nitro groups (N – O), and lastly, the peak at 1 218 cm^{-1} was from carbon to nitrogen bond (C – N).

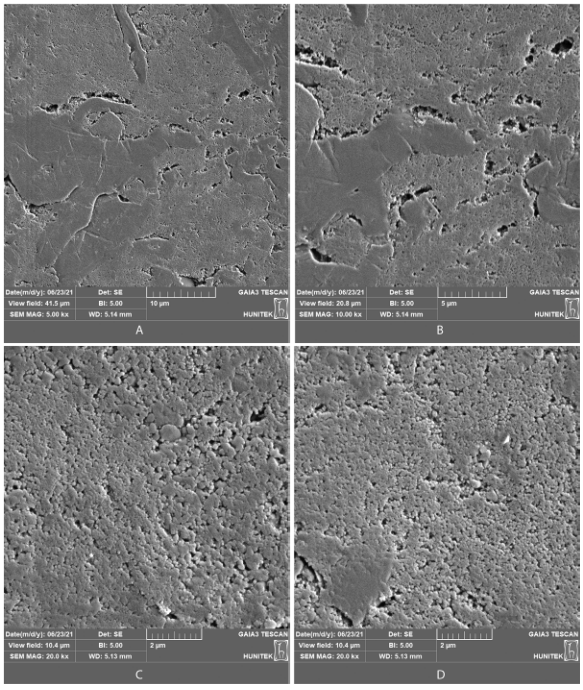

Fig. 3 SEM images of the polymer-coated gold SPR chips: (a) 5.00 kx, (b) 10 kx, (c) 20.0 kx, and (d) 20.0 kx.

The SEM images are given below in Fig. 3. The images of the SMX imprinted polymer-coated chips were taken with SEM. The images were taken from different spots and different magnification values. As seen below, SEM studies showed that the prepared nanofilm spread homogeneously along the chip surface, and the images gave us the results expected from the polymer nanofilm.

In Fig. 4, AFM images are given. Figuire 4(a) belongs to the bare gold chip without coating or surface modification. Figuire 4(b) is from the SMX imprinted polymer-coated gold SPR chip. AFM images showed that the bare gold surface had a depth of 8.5 nm and an average roughness value of 0.52 nm. The SMX-imprinted plasmonic nanosensor surface had a depth of 20.67 nm with an increasing average roughness value (0.76 nm). These results showed that a polymeric nanofilm was successfully formed on the surface.

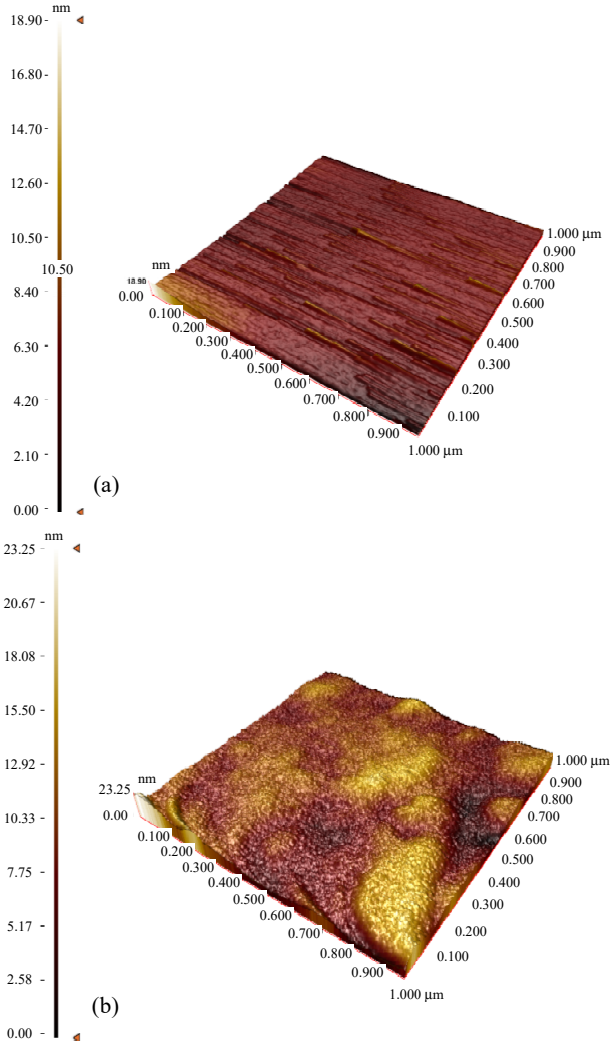

Fig. 4 AFM images of the gold SPR chips: (a) bare gold SPR chip and (b) molecularly imprinted polymer-coated gold SPR chips.

The nanofilm thickness was determined by ellipsometry measurement. Two critical parameters affected nanofilm sensitivity. First, the signal depth depended on the surface plasmon depending on the penetration depth. The second parameter was the high accessibility of the cavity to the nanofilm surface. The nanofilm was preferred within the scope of this study because homogeneously distributed printed regions could be obtained near the surface. Ellipsometry measurements showed that the thickness and roughness increased depending on the nanofilm preparation. For the SMX printed nanofilm, values were (93.2±1.1) nm for the (92.5±1.2) nm unprinted nanofilm, and (32.3±1.3) nm for the allyl mercaptan functionalized nanofilm. The results showed that the nanofilm thickness was relatively thin.

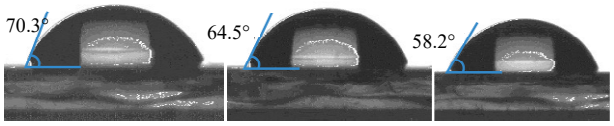

Fig. 5 Contact angle measurement images of the gold SPR chips: (a) bare gold chip, (b) surface modified gold SPR chip, and (c) SMX imprinted polymer film coated gold SPR chips.

A contact angle below 90 ° indicated that the solid surface was suitable for wetting, and there was a liquid spreading over a large area on the solid surface. A contact angle greater than 90 ° usually indicated that the wetting of the surface was unfavourable and that a liquid reduced its contact with the surface and formed a compact liquid droplet. This study performed SMX analysis in aqueous media using the SPR sensor system. The hydrophilic character of the sensor used would directly affect the sensor efficiency. Increasing the sensor surface's hydrophilic character without affecting its selectivity was essential. Contact angle measurements made on bare gold SPR chips, surface modified SPR chips, and SMX imprinted polymer-coated SPR chips and images are given below in Fig. 5. The results for the bare chip [Fig. 5(a)], surface modified chip [Fig. 5(b)], and SMX imprinted polymer-coated chips [Fig. 5(c)] were (70.3±0.42)°, (64.5±0.59)°, and (58.2±0.67)°, respectively. As explained above, the calculated angle was proportional to the surface hydrophilicity in contact angle measurements. In this case, surface modification and polymerization increased the hydrophilic functional groups on the gold SPR chip's surface, which decreased the calculated angle.

3.2 Determination of pH and imprinting factor

The receptor was used in this study made with a non-covalent assembly method. The non-covalent method relies on the complexation between template molecules and functional monomers. In this method, the stronger non-covalent interaction with template-monomer produced stable and high-affinity cavities on molecularly imprinted polymer. If imprinting was made successful, the imprinted polymer would recognize the template molecule via steric/functional group compatibility. This meant the template would bind to cavities in the same manner as pre-complex. Due to that, any changes happening on cavities or the template would affect binding, and pH was a well known factor. Changing pH caused protonation and deprotonation of the template molecule and molecularly imprinted cavities.

This study used sulfamethoxazole (0.025 µg/L) as a template and methacrylic acid as a functional monomer. Both molecules contained many hydrogen bond acceptors and donor sites. The template molecule's primary and secondary amines of SMX, the sulfonyl groups, functional monomer, and carboxylic groups of methacrylic acids could form hydrogen bonds.

The effect of pH (5, 6, 7.4, and 9) on these sites were defined in Fig. 6. All the experiments and measurements were repeated in triplicate. The average of the results obtained was used. According to the graph we acquired from the sensorgram, the maximum SMX adsorption occurred at pH: 7.4. SMX-imprinted polymer (MIP) interaction was mainly made on hydrogen bonding. Due to the

deprotonation effect of high pH, the functional groups of MAA (O – H group) and SMX (primary/ secondary amines) would not make hydrogen bonding. As a result, higher or lower pH values affected ligand binding affinity to the template molecule, and the sensor's selectivity was reduced. Results of pH effects expressed as relative standard deviation (%RSD) was reported less than <1.3, indicating high reproducibility.

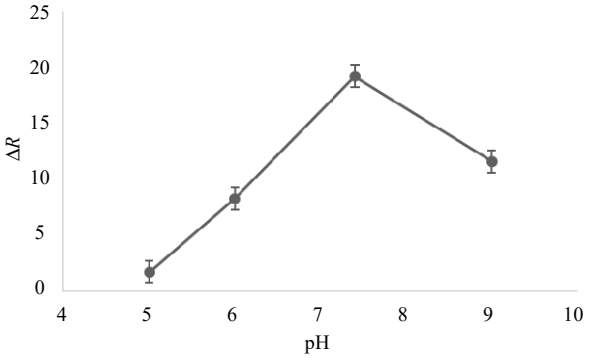

Fig. 6 Effect of pH on adsorption [*C*: 0.025 μg/L, *T*: 25℃, repeated three times (*n* = 3)].

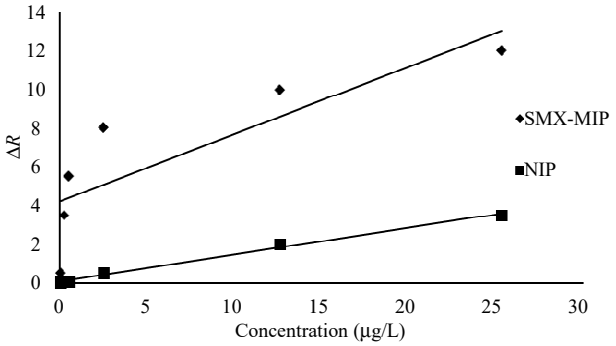

Fig. 7 Imprinting factor (*C*: 0.025 μg/L – 25.2 μg/L, *T*: 25 ℃, and pH: 7.4).

To evaluate the imprinting effect on SMX adsorption, we investigated non-imprinted polymer-coated (NIP) SPR chips and SMX imprinted (SMX-MIP) SPR chips with different SMX concentrations (0.025 μg/L – 25.2 μg/L) in Fig. 7. The adsorption on the surface of the non-imprinted polymer-coated chips was calculated as 3.5, resulting from most hydrogen bonding between SMX and the functional groups. The SMX imprinted polymer coating chip adsorption was calculated as 12, which meant molecular imprinting increased the adsorption of SMX on the surface of the chips. According to these calculations, imprinting factor (IF) was calculated as: ΔR(MIP)/ΔR(NIP) = 12/3.5 = 3.4. This result meant imprinting was done successfully and increased affinity to SMX molecule for 3.4 folds. The imprinting created geometrically compatible cavities on the template, and this geometrical compatibility was the result of the difference of adsorption between these two chips.

3.3 Adsorption and kinetic studies

Real-time SMX adsorption studies were made by SMX imprinted polymer-coated SPR nanosensor chips. The study was made with a concentration difference between 0.025μg/L – 253.2 μg/L SMX. We used a phosphate buffer at 7.4 pH to equilibrate the chips for this study. After the solutions were given to SPR chips, the SPR view application calculated the results. These adsorptions, desorption, and regeneration processes were finished within 20 minutes. The acquired sensorgrams and calibration curves we draw are given below in Fig. 8. LOD and LOQ values were calculated with 3 s/m and 10 s/m methods, and the results were found to be 0.001 1 μg/L for LOD and 0.003 4 μg/L for LOQ. The nanosensor we developed could detect SMX between 0.025 μg/L and 2.5 μg/L and 12.6 μg/L and 253.2 μg/L concentration ranges with 94% and 97% accuracy. Since the concentrations of SMX and other sulfonamides were very low in both food products and environmental waters, the determination of these molecules at low concentrations was rather edematous. Table 1 shows the SMX analysis methods using different techniques. As can be seen from the table, the LOD value of the MIP sensor prepared was much lower than those of other methods.

Kinetic analysis was made under pseudo-first-order conditions (assuming that the concentration of the free analyte was kept constant in the flow cell). The adsorption can be defined by

$$\mathrm{d}\Delta R / \mathrm{d}t = k_a C \Delta R_{\max} - (k_a C + k_d) . \quad (1)$$

With this equation, we calculated the kinetic parameter. Calculated parameters are given below in

Table 2. The rate constants and equilibrium constants of adsorption of sulfamethoxazole by designed nanosensor gave information about the interaction between the target molecule and the designed nanosensor and also the strength of association. As seen in Table 2, the association rate constant (0.27 L/µgs) was more than the disassociation rate constant (0.04 1/s), and the association equilibrium constant (6.75 L/µg) was more than the dissociation equilibrium constant (0.15 µg/L). These data represent the high affinity of sulfamethoxazole molecules to the designed nanosensor.

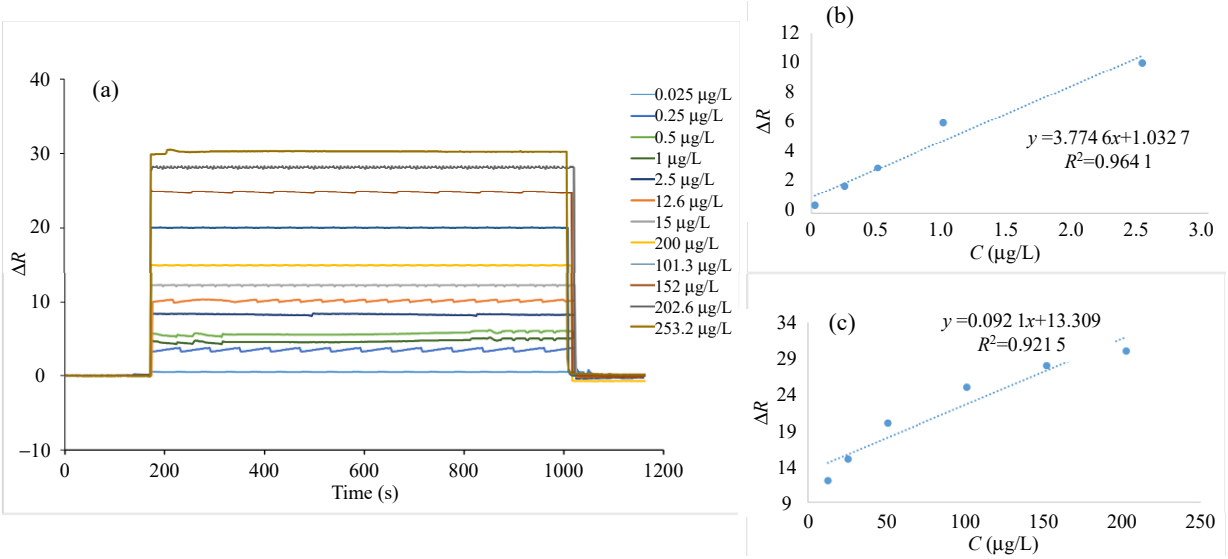

Fig. 8 Response sensogram and calibration graph: (a) real-time SPR chip response sensograms for SMX (*C*: 0.025253.2 µg/L – 253.2 µg/L, *T*: 25 ˚C, and pH: 7.4), (b) calibration graph of 0.025 µg/L – 2.5 µg/L SMX, and (c) calibration graph of 12.6 µg/L – 253.2 µg/L SMX concentration.

Table 1 Recent SMX sensor studies with different methods and the LOD values of these studies.

Sensor	Method	Competitive agents	Analysis range	LOD	Ref.
Electrochemical-DVP	MWCNT-Pbnc/SPE	-	0.1µmol·L^{-1} – 10.0 µmol·L^{-1}	38 nm/L	[54]
Electrochemical	MWCNT-SbNPs-Parafin	Trimethoprim	0.1µmol·L^{-1} – 0.7 µmol·L^{-1}	6.1 µg/L	[55]
Electrochemical	MIP/BDD Elektrot	Sulfadimethoxine, sulfadiazine, Sulfafurazole	0.1 mM – 100 mM	24.1 nM	[56]
Electrochemical-Bio	Tyrosin-AuNPs-SPCEs		20 µM – 0.2 mM	(22.6±2.1) µM	[57]
Electrochemical	G-C3N4/ZnO/GCE	Ascorbic acid, uric acid, dopamine, Trimethoprim, phenazopyridine, Sulfadiazine, sulfamethizole, glucose, and H_2O_2	20 nM – 1.1 mM	0.0066 µM	[58]
Bioassay	B. Licheniformis	-	-	77 µg/L	[59]
Fluorescent sensor	GQD-SMIP	Sulfadiazine, sulfamerazine, sulfamethazine, Sulfasalazine sulfapyridine	1 µM – 100 µM	1 µM	[60]
SPR	CNTs	Dopamine, ascorbic acid, uric acid, glucose, citric acid	0 – 200 µM	0.89 µM	[61]
SPR	Entrapped tyrosinase enzyme in polyacrylamide gel	Dopamine, ascorbic acid, uric acid, glucose, citric acid	0 – 200 µM	1.137 µM	[61]
SPR	SMX-imprinted MAA-EGDMA-HEMA polymer	Amoxycillin, cephalexin	0.025µg/L – 253.2 µg/L	0.001 1 µg/L	This study

Table 2 Equilibrium and binding coefficients.

Association kinetics analysis		Equilibrium analysis (Scatchard)	
k_a (L/μgs)	0.27	ΔR_{max} (μg/cm^2)	30.6
k_d (1/s)	0.04	K_A (L/μg)	0.55
K_A (L/μg)	6.75	K_D (μg/L)	1.8
K_D (μg/L)	0.15	R^2	0.89
R^2	0.91		

3.4 Adsorption characteristics and isotherms

To determine adsorption characteristic of the SMX and nanofilm on the SPR chip, three different isotherm models used Langmuir, Freundlich, and Langmuir-Freundlich. We used the equations given below for calculations.

Langmuir:

$$\Delta R = (\Delta R_{max} C / K_D + C) .$$

Freundlich:

$$\Delta R = \Delta R_{max} C^{1/n} .$$

Langmuir-Freundlich:

$$\Delta R = (\Delta R_{max} C^{1/n}) + C^{1/n} .$$

Calculated results are given in Table 3. The result showed us that the SMX-nanofilm adsorption characteristic was closer to the Freundlich model. That meant adsorption was heterogeneous, binding sites were not energetically equal, and more than one molecule could bind to one site.

Table 3 Adsorption isotherm models.

Langmuir		Freundlich		Langmuir-Freundlich	
ΔR_{max}	14.2	ΔR_{max}	33.3	ΔR_{max}	43.4
K_D	0.003	$1/n$	0.31	$1/n$	0.31
K_A	294	R^2	0.99	K_D	0.022
R^2	0.97			K_A	45.5
				R^2	0.84

3.5 Selectivity

One of the most critical features of the sensors was that although they showed high selectivity for the target molecule, they showed very low selectivity towards other molecules in the environment. To test the sensor selectivity, selectivity studies were carried out by adding other antibiotics likely to be present in the medium.

For selectivity studies, we used two different antibiotics: amoxicillin and cephalexin. Amoxicillin and cephalexin were widely beta-lactam antibiotics used to treat infections caused by gram-positive bacteria. The selected molecules were chosen according to their close structural similarity with the target molecule and their probability of being in the same environment as the target molecule. Each antibiotic was given to the sensor with a concentration equal to 25.3 μg/L. The acquired sensorgram is given in Fig. 9, and the calculated parameters are given in the table in Table 4.

Table 4 Specificity coefficients of SMX-MIP and NIP nanofilms.

	MIP		NIP		
	ΔR	k	ΔR	k	k'
SMX	12.3		2.3		
Amoxicillin	2.1	5.7	5.1	0.45	12.7
Cephalexin	5.3	2.3	3.5	0.66	3.4

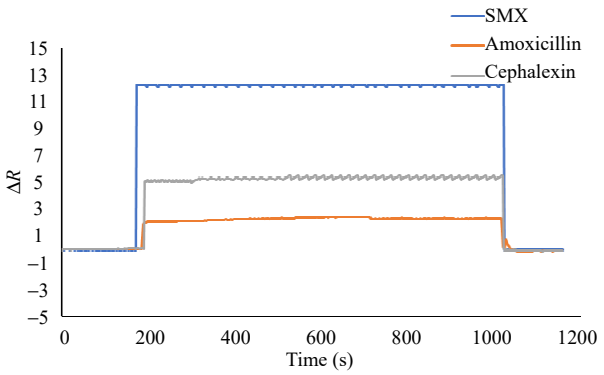

Fig. 9 Response of the sensor to different antibiotics (C: 25.3 μg/L, T: 25 ℃, and pH: 7.4).

As seen in the Table 4, the calculated selectivity constants of sulfamethoxazole concerning amoxicillin and cephalexin were 5.7 and 2.3, respectively; also, for non-imprinted nanosensors, these values were 0.45 and 0.66, respectively. The calculated relative selectivity constants of sulfamethoxazole (12.7 and 3.4) indicated the imprinting efficiency of sulfamethoxazole for amoxicillin and cephalexin. As a result, the response signal of imprinting nanosensor for sulfamethoxazole was higher than those of other antibiotics. On the other hand, the selectivity of the non-imprinted chip SMX was lowest compared to

the other antibiotics. The selectivity of SMX was increased nearly fivefold with amoxicillin and three-fold for cephalexin. This meant the molecular imprinted polymer-coated chips held more selectivity for SMX. These results showed us SMX imprinting was done successfully and increased the selectivity to SMX in imprinted polymer-coated chips in Fig. 9.

3.5 Reusability and storability

The reusability and storability of the imprinted chips were investigated in Fig. 10. We ran five continuous analysis cycles [repeated three times (n=3)] for the reusability experiment with 25.3 µg/L SMX. After doing five continuous equilibrium adsorption-desorption cycles in Fig. 10(a), the reusability experiment showed the nanosensors hold analysis capability even after five continuous analysis cycles.

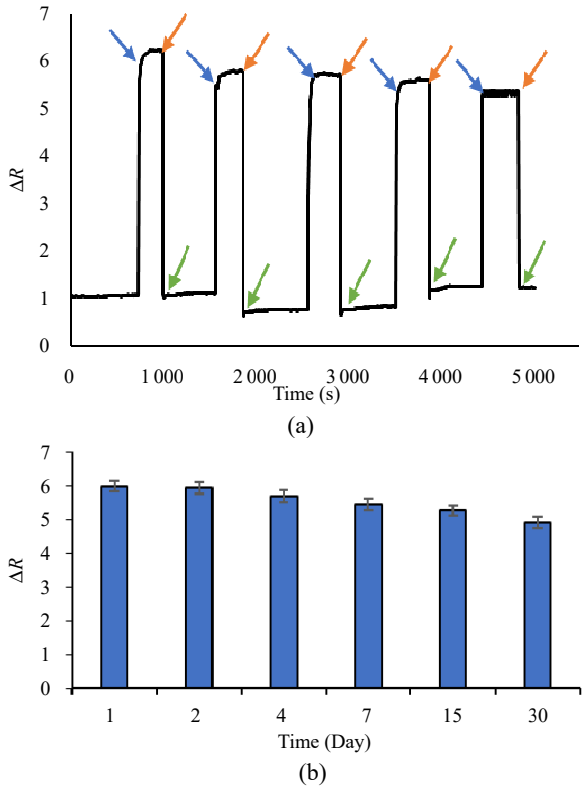

Fig. 10 Repeatability and storability: (a) repeatability, the measurement was repeated three times (n=3) with five replicates (C: 25.3 µg/L, T: 25 ˚C, and pH: 7.4, blue arrow: equilibration, red arrow: adsorption, green arrow: regeneration) and (b) storability, sensogram acquired from SMX analysis on different dates [C: 25.3 µg/L, T: 25 ˚C, and pH: 7.4, repeated three times (n=3)].

For storability, we ran the experiment at different dates ranging from one day to one month in Fig. 10(b) to investigate the storage durability of the sensor. We selected the first day, second day, fourth day, first week, second week, and one month after its fabrication (storage condition: 4 ˚C in 7.4 pH of buffer solution). Precision studies determined the reproducibility studies of the system. Signal response reproducibility studies of the nanosensor were evaluated statistically for intraday tests (five replicates with three groups), and reproducibility accuracy was verified by calculating the %RSD. Results of intraday experiments, expressed as %RSD, were reported less than 1.3 indicating high reproducibility. According to the results, even after the one month, the sensor held great affinity to SMX. Reusability and storability experiment showed us that our sensor held excellent reusability and storability, which was the desired property for a sensor because reusing the same sensor chip meant lower cost and less labor.

3.6 Real sample analysis

We used a newly developed SPR sensor to detect SMX in the spiked commercial milk samples. Furthermore, the same experiment was done with the UV-VIS method, which was recommended for SMX analysis. Before analysis, we prepared milk samples. First, two commercial milk samples were centrifuged and filtered to remove the fat layer and diluted to a water 1:10 ratio. After this step, we analyzed chips, but the UV-VIS spectrometer did not give us results because of protein interference in the milk samples. To continue the determination of SMX with UV-VIS, we did an extra step of protein hydrolysis with the enzyme (trypsin) in Table 5. As seen below, analysis done with chips had a more effective recovery rate. Interference caused by biological species in milk samples was unavoidable. When comparing recovery obtained here and in the UV-VIS method, the availability of matrix effects and interferences in the commercial milk sample was more dominant in lower SMX recovery.

Increasing SMX concentration caused a decrease in matrix and interference effects, and accordingly, the recovery rate increased. It was probably best to use molecularly imprinted polymers (MIPs) with predetermined selectivity for an imprinted template to eliminate the interfering effect. MIP based nanosensors that mimic the key-lock fit were prepared according to the shape, size, geometry and functional groups specific to the target molecule. MIP-based nanosensors were specific to the target molecule matrix and minimized matrix and interference effects. Additionally, the preparation of the samples was less laborious and costly than the UV-VIS method.

Table 5 Real-time SMX analysis and comparison to UV method.

	Foud (μM)				Recovery (%)	
	SPR		UV		SPR	UV
Added SMX (μM)	Sample 1	Sample 2	Sample 1	Sample 2		
2.5	2.44	2.42	1.8	1.9	97.2	74
25.3	24.8	25	20.6	22	98.4	84.2
202.6	201.5	201.8	191	190	99.5	94.0
253.2	249.1	251.5	238	234.2	98.8	93.2

4. Conclusions

Antibiotics are essential for health, but they also have many disadvantages, such as environmental and food pollutants. Consuming antibiotic residues can cause serious health problems; antibiotic resistance is another problem. SMX is often used as a food additive in livestock to increase production. In this study, the SPR nanosensor was prepared for the real-time determination of SMX. SPR nanosensors were characterized by contact angle measurements, atomic force microscopy, scanning electron microscopy, and FTIR. Scatchard, Langmuir, Freundlich, and Freundlich-Langmuir models were used for binding, equilibrium and adsorption kinetics. Freundlich adsorption model was determined the most acceptable model for an SMX imprinted SPR sensor. Accurate and rapid determination of SMX in complex environments is a significant challenge. When the literature is examined, it is seen that SMX sensor studies are limited in Table 1. As shown in Table 5, different methods can detect and determine SMX. The table is prepared with different parameters such as working range, detection limit, analysis time, and competitor agents. Each of the studies has advantages and disadvantages. When the sensor studies are examined, it is seen that the majority of them are electrochemically based, and it is seen that the LOD values are pretty high. SMX sensor studies based on SPR have not been found in the literature. The SMX-imprinted MAA-EGDMA-HEMA polymer film sensor system we prepared was an exciting and new method. With this technique, it had been possible to perform simultaneous analysis of SMX at low detection limits (0.001 1 μg/L for LOD and 0.003 4 μg/L for LOQ) in a short time. Moreover, SMX was determined directly by the designed SPR biosensor in high precision and selectivity. The developed imprinting nanosensor observed a high selectivity at low concentrations (0.025 μg/L – 2.5 μg/L). Using polymeric nanofilms based on molecular imprinting made the nanosensor more selective and sensitive in SMX determination. As a result, the determination of SMX was developed, which can be used for both research and industrial applications to get better results such as faster, cheaper, and compact optical-based nanosensor systems.

Acknowledgment

The authors thank Prof. Dr Adil Denizli for his expertise and assistance throughout our study.

References

[1] E. Y. Klein, T. P. van Boeckel, E. M. Martinez, S. Pant, S. Gandra, S. A. Levin, *et al*., "Global increase and geographic convergence in antibiotic consumption between 2000 and 2015," *Proceedings of the National Academy of Sciences of the United States of America*, 2018, 115(15): E3463–E3470.

[2] G. Busch, B. Kassas, M. A. Palma, and A. Risius, "Perceptions of antibiotic use in livestock farming in Germany, Italy and the United States," *Livestock Science*, 2020, 241: 104251.

[3] X. Yin, N. M. M'ikanatha, E. Nyirabahizi, P. F. McDermott, and H. Tate, "Antimicrobial resistance in non-typhoidal salmonella from retail poultry meat by antibiotic usage-related production claims – United States, 2008–2017," *International Journal of Food Microbiology*, 2021, 342: 109044.

[4] E. U. Ahiwe, T. T. Tedeschi Dos Santos, H. Graham, and P. A. Iji, "Can probiotic or prebiotic yeast (Saccharomyces cerevisiae) serve as alternatives to in-feed antibiotics for healthy or disease-challenged broiler chickens?: a review," *Journal of Applied Poultry Research*, 2021, 30(3): 100164.

[5] L. C. Scott, M. J. Wilson, S. M. Esser, N. L. Lee, M. E. Wheeler, A. Aubee, *et al*., "Assessing visitor use impact on antibiotic resistant bacteria and antibiotic resistance genes in soil and water environments of Rocky Mountain National Park," *Science of The Total Environment*, 2021, 785: 147122.

[6] A. Serra-Compte, M. G. Pikkemaat, A. Elferink, D. Almeida, J. Diogène, J. A. Campillo, *et al*., "Combining an effect-based methodology with chemical analysis for antibiotics determination in wastewater and receiving freshwater and marine environment," *Environmental Pollution*, 2021, 271: 116313.

[7] Z. E. Menkem, B. L. Ngangom, S. S. A. Tamunjoh, and F. F. Boyom, "Antibiotic residues in food animals: public health concern," *Acta Ecologica Sinica*, 2019, 39(5): 411–415.

[8] L. M. Chiesa, L. DeCastelli, M. Nobile, F. Martucci, G. Mosconi, M. Fontana, *et al*., "Analysis of antibiotic residues in raw bovine milk and their impact toward food safety and on milk starter cultures in cheese-making process," *LWT*, 2020, 131: 109783.

[9] M. Bacanlı and N. Başaran, "Importance of antibiotic residues in animal food," *Food and Chemical Toxicology*, 2019, 125: 462–466.

[10] H. Wu, Y. Ma, X. Peng, W. Qiu, L. Kong, B. Ren, *et al*., "Antibiotic-induced dysbiosis of the rat oral and gut microbiota and resistance to salmonella," *Archives of Oral Biology*, 2020, 114: 104730.

[11] A. Kim, N. Kim, H. J. Roh, W. K. Chun, D. T. Ho, Y. Lee, *et al*., "Administration of antibiotics can cause dysbiosis in fish gut," *Aquaculture*, 2019, 512: 734330.

[12] M. Li, Z. K. Lu, D. J. Amrol, J. R. Mann, J. W. Hardin, J. Yuan, *et al*., "Antibiotic exposure and the risk of food allergy: evidence in the US medicaid pediatric population," *The Journal of Allergy and Clinical Immunology: In Practice*, 2019, 7(2): 492–499.

[13] R. W. Steele, R. Warrier, P. J. Unkel, B. J. Foch, R. F. Howes, S. Shah, *et al*., "Colonization with antibiotic-resistant streptococcus pneumoniae in children with sickle cell disease," *The Journal of Pediatrics*, 1996, 128(4): 531–535.

[14] L. Papst, B. Beovic, C. Pulcini, E. Durante-Mangoni, J. Rodríguez-Baño, K. S. Kaye, *et al*., "Antibiotic treatment of infections caused by carbapenem-resistant Gram-negative bacilli: an international ESCMID cross-sectional survey among infectious diseases specialists practicing in large hospitals," *Clinical Microbiology and Infection*, 2018, 24(10): 1070–1076.

[15] C. C. R. F. da Cunha, M. G. Freitas, D. A. da Silva Rodrigues, A. L. C. de Barros, M. C. Ribeiro, A. L. Sanson, *et al*., "Low-temperature partitioning extraction followed by liquid chromatography tandem mass spectrometry determination of multiclass antibiotics in solid and soluble wastewater fractions," *Journal of Chromatography A*, 2021, 1650: 462256.

[16] F. Tasci, H. S. Canbay, and M. Doganturk, "Determination of antibiotics and their metabolites in milk by liquid chromatography-tandem mass spectrometry method," *Food Control*, 2021, 127: 108147.

[17] E. Comini, "Metal oxides nanowires chemical/gas sensors: recent advances," *Materials Today Advances*, 2020, 7: 100099.

[18] M. Jalilzadeh, D. Çimen, E. Özgür, C. Esen, and A. Denizli, "Design and preparation of imprinted surface plasmon resonance (SPR) nanosensor for detection of Zn(II) ions," *Journal of Macromolecular Science, Part A*, 2019, 56(9): 877–886.

[19] Z. Rasouli, M. Maeder, and H. Abdollahi, "Using chemical modeling for designing of optimal pH sensor based on analytical sensitivity enhancement," *Microchemical Journal*, 2021, 168: 106450.

[20] Y. Kojima, T. Kawashima, K. Noborio, K. Kamiya, and R. Horton, "A dual-probe heat pulse-based sensor that simultaneously determines soil thermal properties, soil water content and soil water matric potential," *Computers and Electronics in Agriculture*, 2021, 188: 106331.

[21] J. S. Kim, Y. So, S. Lee, C. Pang, W. Park, and S. Chun, "Uniform pressure responses for nanomaterials-based biological on-skin flexible pressure sensor array," *Carbon*, 2021, 181: 169–176.

[22] Q. D. Huang, C. H. Lv, X. L. Yuan, M. He, J. P. Lai,

and H. Sun, "A novel fluorescent optical fiber sensor for highly selective detection of antibiotic ciprofloxacin based on replaceable molecularly imprinted nanoparticles composite hydrogel detector," *Sensors and Actuators B: Chemical*, 2021, 328: 129000.

[23] R. Xie, P. Yang, J. Liu, X. Zou, Y. Tan, X. Wang, *et al*., "Lanthanide-functionalized metal-organic frameworks based ratiometric fluorescent sensor array for identification and determination of antibiotics," *Talanta*, 2021, 231: 122366.

[24] B. Öndeş, F. Akpınar, M. Uygun, M. Muti, and D. A. Uygun, "High stability potentiometric urea biosensor based on enzyme attached nanoparticles," *Microchemical Journal*, 2021, 160: 105667.

[25] Z. Zhang, O. Niwa, S. Shiba, S. Tokito, K. Nagamine, S. Ishikawa, *et al*., "Electrochemical enzyme biosensor for carnitine detection based on cathodic stripping voltammetry," *Sensors and Actuators B: Chemical*, 2020, 321: 128473.

[26] X. Zhao, X. Dai, S. Zhao, X. Cui, T. Gong, Z. Song, *et al*., "Aptamer-based fluorescent sensors for the detection of cancer biomarkers," *Spectrochimica Acta Part A: Molecular and Biomolecular Spectroscopy*, 2021, 247: 119038.

[27] X. Wang, X. Wang, Y. Liu, T. Chu, Y. Li, C. Dai, *et al*., "Surface plasma enhanced fluorescence combined aptamer sensor based on silica modified silver nanoparticles for signal amplification detection of cholic acid," *Microchemical Journal,* 2021, 168: 106524.

[28] A. Wang, X. You, H. Liu, J. Zhou, Y. Chen, C. Zhang, *et al*., "Development of a label free electrochemical sensor based on a sensitive monoclonal antibody for the detection of tiamulin," *Food Chemistry*, 2022, 366: 130573.

[29] H. Yang, Q. Zhang, X. Liu, Y. Yang, Y. Yang, M. Liu, *et al*., "Antibody-biotin-streptavidin-horseradish peroxidase (HRP) sensor for rapid and ultra-sensitive detection of fumonisins," *Food Chemistry*, 2020, 316: 126356.

[30] E. Özgür, Y. Saylan, N. Bereli, D. Türkmen, and A. Denizli, "Molecularly imprinted polymer integrated plasmonic nanosensor for cocaine detection," *Journal of Biomaterials Science*, *Polymer Edition*, 2020, 31(9): 1211–1222.

[31] S. Akgönüllü, C. Armutcu, and A. Denizli, "Molecularly imprinted polymer film based plasmonic sensors for detection of ochratoxin A in dried fig," *Polymer Bulletin*, 2021, DOI: doi.org/10.1007/s00289-021-03699-6.

[32] P. Teengam, N. Nisab, N. Chuaypen, P. Tangkijvanich, T. Vilaivan, and O. Chailapakul, "Fluorescent paper-based DNA sensor using pyrrolidinyl peptide nucleic acids for hepatitis C virus detection," *Biosensors and Bioelectronics*, 2021, 189: 113381.

[33] S. T. Rajendran, K. Huszno, G. Dębowski, I. Sotres, T. Ruzgas, A. Boisen, *et al*., "Tissue-based biosensor for monitoring the antioxidant effect of orally administered drugs in the intestine," *Bioelectrochemistry*, 2021, 138: 107720.

[34] F. Guo and H. Liu, "Impact of heterotrophic denitrification on BOD detection of the nitrate-containing wastewater using microbial fuel cell-based biosensors," *Chemical Engineering Journal*, 2020, 394: 125042.

[35] S. Lí and G. A. Drago, "Bioconjugation and stabilisation of biomolecules in biosensors," *Essays in Biochemistry*, 2016, 60(1): 59–68.

[36] A. D. Mcconnell, V. Spasojevich, J. L. Macomber, I. P. Krapf, A. Chen, J. C. Sheffer, *et al*., "An integrated approach to extreme thermostabilization and affinity maturation of an antibody," *Protein Engineering, Design and Selection*, 2013, 26(2): 151–164.

[37] P. V. Iyer and L. Ananthanarayan, "Enzyme stability and stabilization-aqueous and non-aqueous environment," *Process Biochemistry*, 2008, 43(10): 1019–1032.

[38] S. Akgönüllü, H. Yavuz, and A. Denizli, "SPR nanosensor based on molecularly imprinted polymer film with gold nanoparticles for sensitive detection of aflatoxin B1," *Talanta*, 2020, 219: 121219.

[39] S. Akgönüllü, H. Yavuz, A. Denizli, M. García, and A. C. Grijalba, "Development of gold nanoparticles decorated molecularly imprinted-based plasmonic sensor for the detection of aflatoxin m1 in milk samples," *Chemosensors*, 2021, 9(12): 363.

[40] R. Ahmad, N. Griffete, A. Lamouri, N. Felidj, M. M. Chehimi, and C. Mangeney, "Nanocomposites of gold nanoparticles@molecularly imprinted polymers: chemistry, processing, and applications in sensors," *Chemistry of Materials*, 2015, 27(16): 5464–5478.

[41] S. Balbinot, A. M. Srivastav, J. Vidic, I. Abdulhalim, and M. Manzano, "Plasmonic biosensors for food control," *Trends in Food Science & Technology*, 2021, 111: 128–140.

[42] Q. Liu, H. Xie, J. Liu, J. Kong, and X. Zhang, "A novel electrochemical biosensor for lung cancer-related gene detection based on copper ferrite-enhanced photoinitiated chain-growth amplification," *Analytica Chimica Acta*, 2021, 1179: 338843.

[43] L. Hu, B. Gong, N. Jiang, Y. Li, and Y. Wu, "Electrochemical biosensor for cytokinins based on the CHASE domain of arabidopsis histidine kinases 4," *Bioelectrochemistry*, 2021, 141: 107872.

[44] W. Wu, J. Huang, L. Ding, H. Lin, S. Yu, F. Yuan, *et al*., "A real-time and highly sensitive fiber optic biosensor based on the carbon quantum dots for nitric oxide detection," *Journal of Photochemistry and Photobiology A: Chemistry*, 2021, 405: 112963.

[45] V. Yesudasu, H. S. Pradhan, and R. J. Pandya, "Recent progress in surface plasmon resonance based sensors: a comprehensive review," *Heliyon*, 2021, 7(3): e06321.
[46] J. Wollschlaeger and K. O. Möller, "Ocean in situ sensors: new developments in biological sensors," *Challenges and Innovations in Ocean In Situ Sensors: Measuring Inner Ocean Processes and Health in the Digital Age*, 2019: 81–116.
[47] L. Zhang, J. Liu, and E. Wang, "A new method for studying the interaction between chlorpromazine and phospholipid bilayer," *Biochemical and Biophysical Research Communications*, 2008, 373(2): 202–205.
[48] L. Quan, D. Wei, X. Jiang, Y. Liu, Z. Li, N. Li, *et al*., "Resurveying the tris buffer solution: The specific interaction between tris (hydroxymethyl) aminomethane and lysozyme," *Analytical Biochemistry*, 2008, 378(2): 144–150.
[49] S. Michaelis, J. Wegener, and R. Robelek, "Label-free monitoring of cell-based assays: combining impedance analysis with SPR for multiparametric cell profiling," *Biosensors and Bioelectronics*, 2013, 49: 63–70.
[50] A. Arif Topçu, E. Özgür, F. Yılmaz, N. Bereli, and A. Denizli, "Real time monitoring and label free creatinine detection with artificial receptors," *Materials Science and Engineering: B*, 2019, 244: 6–11.
[51] Z. Mao, J. Zhao, J. Chen, X. Hu, K. Koh, and H. Chen, "A simple and direct SPR platform combining three-in-one multifunctional peptides for ultra-sensitive detection of PD-L1 exosomes," *Sensors and Actuators B: Chemical*, 2021, 346: 130496.
[52] G. Beketov, O. Shynkarenko, and M. Apatska, "Towards improving ELISA surfaces: SPR assessment of polystyrene modification efficiency for promoting immobilization of biomolecules," *Analytical Biochemistry*, 2021, 618: 114101.
[53] S. Wang, H. Yang, H. Zhang, F. Yang, M. Zhou, C. Jia, *et al*., "A surface plasmon resonance-based system to genotype human papillomavirus," *Cancer Genetics and Cytogenetics*, 2010, 200(2): 100–105.
[54] L. F. Sgobbi, C. A. Razzino, and S. A. S. Machado, "A disposable electrochemical sensor for simultaneous detection of sulfamethoxazole and trimethoprim antibiotics in urine based on multiwalled nanotubes decorated with prussian blue nanocubes modified screen-printed electrode," *Electrochimica Acta*, 2016, 191: 1010–1017.
[55] I. Cesarino, V. Cesarino, and M. R. V. Lanza, "Carbon nanotubes modified with antimony nanoparticles in a paraffin composite electrode: simultaneous determination of sulfamethoxazole and trimethoprim," *Sensors and Actuators B: Chemical*, 2013, 188: 1293–1299.
[56] Y. Zhao, F. Yuan, X. Quan, H. Yu, S. Chen, H. Zhao, *et al*., "An electrochemical sensor for selective determination of sulfamethoxazole in surface water using a molecularly imprinted polymer modified BDD electrode," *Analytical Methods*, 2015, 7(6): 2693–2698.
[57] L. del Torno-de Román, M. Asunción Alonso-Lomillo, O. Domínguez-Renedo, and M. J. Arcos-Martínez, "Tyrosinase based biosensor for the electrochemical determination of sulfamethoxazole," *Sensors and Actuators B: Chemical*, 2016, 227: 48–53.
[58] P. Balasubramanian, R. Settu, S. M. Chen, and T. W. Chen, "Voltammetric sensing of sulfamethoxazole using a glassy carbon electrode modified with a graphitic carbon nitride and zinc oxide nanocomposite," *Microchimica Acta*, 2018, 185(8): 396–404.
[59] M. Tumini, O. G. Nagel, and R. L. Althaus, "Five-assay microbiological system for the screening of antibiotic residues," *Revista Argentina de Microbiología*, 2019, 51(4): 345–353.
[60] T. H. Le, H. J. Lee, J. H. Kim, and S. J. Park, "Highly selective fluorescence sensor based on graphene quantum dots for sulfamethoxazole determination," *Materials*, 2020, 13(11): 2521.
[61] A. Pathak, S. Parveen, and B. D. Gupta, "Fibre optic SPR sensor using functionalized CNTs for the detection of SMX: comparison with enzymatic approach," *Plasmonics*, 2018,13(1): 189–202.